Protein Regulation Strategies of Mouse Spleen in Response to Babesia Microti Infection

Xiaomin Xue
Hebei Normal University
Shuguang Ren
Hebei Medical University Fourth Affiliated Hospital and Hebei Provincial Tumor Hospital
Abolfazl Masoudi
Hebei Normal University
Yuhong Hu
Hebei Normal University
Xiaoshuang Wang
Hebei Normal University
Hongxia Li
Hebei Normal University
Xiaojing Zhang
Hebei Normal University
Minjing Wang
Hebei Normal University
Hui Wang
Hebei Normal University
Jing-Ze Liu (liujingze@hebtu.edu.cn)
Hebei Normal University

Research

Keywords: Babesia microti, spleen, quantitative proteomics, phosphorylation, immune

Posted Date: September 25th, 2020

DOI: https://doi.org/10.21203/rs.3.rs-81340/v1

Version of Record: A version of this preprint was published on January 19th, 2021. See the published version at https://doi.org/10.1186/s13071-020-04574-5.

Abstract

Background

Babesia is a protozoan parasite in red blood cells of some vertebrates. Some species of *Babesia* can cause zoonoses and cause great harm. As the largest immune organ in mammals, the spleen plays an important role in defending against *Babesia* infection. When infected with *Babesia*, the spleen is seriously injured, but it still actively initiates immunomodulatory responses.

Methods

In order to explore the molecular mechanisms underlying the immune regulation and self-repair of the spleen in response to infection, this study used data-independent acquisition (DIA) quantitative proteomics to analyse changes in expression levels of global proteins and changes in phosphorylation modification in spleen tissue after *Babesia microti* infection in mice.

Results

After the mice were infected with *B. microti*, their spleen were seriously damaged.Using bioinfor-matics methods to analyze the dynamic changes of a large number of proteins, we found that spleen still initiated immune response to deal with the infection, in which immune-related proteins played an important role, including CTSD, IFI44, ILF2, ILF, and STAT5A. In addition, some proteins related to iron metabolism were also involved in the repair of spleen against *B. microti* infection, including serotransferrin, lactoferrin, TfR1, and GCL. At the same time, the expression and phosphorylation of proteins related to the growth and development of the spleen also changed, including PKC-δ and MAPK3/1, Grb2, and PAK2.

Conclusions

Immune-related proteins, iron metabolism-related proteins and growth and development-related proteins play an important important role in the regulation of spleen injury and maintenance of homeostasis. This study will provide important bases for the diagnosis and treatment of babesiosis.

Background

Babesia is a blood parasitic protozoan [1]. Hosts infected with *Babesia* develop babesiosis. *Babesia* is mainly transmitted by blood transfusion, placenta and ticks [2,3]. People with infection exhibit symptoms such as fever, anaemia, haemoglobinuria, while the severe ones were accompanied by multiple organ damage [4]. *Babesia microti*, the focus of this study, is a parasite mainly in mice and is also one of the important pathogens of human babesiosis [5].

The spleen is the largest immune system organ in the body. It is very important for the clearance of parasites. People with splenic insufficiency or who have undergone splenectomy will experience more

severe diseases after suffering from babesiosis [6]. *Babesia* infection results in severe spleen injury. However, the injured spleen will still actively initiate immunomodulatory responses during self-repair. The spleen contains a large amount of B lymphocytes and macrophages and can also produce immunoglobulins and complements that exert immune functions [7]. Initiation and operation of these immunomodulatory functions and repair mechanisms of the spleen are achieved through coordination among many proteins. These proteins exert their functions through changes in their expression levels and post-translational modifications. To elucidate the molecular regulatory mechanisms of immune responses and self-repair exhibited by the spleen during different stages of *Babesia* infection, this study used data-independent acquisition (DIA) [8] quantitative proteomics to comprehensively analyse changes in expression levels and phosphorylation modifications of proteins in mouse spleen tissues during different stages of *B. microti* infection. To our knowledge, this is the first proteomics study on mammalian spleen after *Babesia* infection. This study showed that expression levels of immune-, iron metabolism-, and growth and development-related proteins in mouse spleen tissues changed after *Babesia* infection. In addition, phosphorylation modifications of these proteins also changed. These study results may provide theoretical bases for analyses of how the spleen perceives *Babesia* infection stress and resists *Babesia* infection and theoretical bases for the effective detection, diagnosis, and treatment of babesiosis.

Methods

Dissection of mouse spleen and sample preparation

B. microti (ATCC PRA-99^{TM}) was obtained from the Institute of Laboratory Animal Sciences, Chinese Academy of Medical Sciences. Female BALB/c mice were raised to 6 weeks of age, and then, the mice received intraperitoneal injection of 150 μl of *B. microti*-infected erythrocytes (1.8×10^7) [9]. After 5 d, 8 d, 11 d, and 19 d, mice infected with *B. microti* were anaesthetized and euthanized, and the spleen was dissected. The spleen of normal mice was used as the negative control. Spleen tissue samples (2 mm^3) were immediately placed in 4% glutaraldehyde fixative for storage and used for subsequent transmission electron microscopy (TEM) analysis. The remaining tissues were rapidly frozen at –80°C for subsequent proteomics studies. The infection rate was calculated via blood smear. All experimental procedures were approved by the Animal Ethics Committee of Hebei Normal University (No. 165031). The involved animal feeding and material collection procedures were all performed in the level 2 biosafety laboratory in The Fourth Hospital of Hebei Medical University.Preparation of TEM samples and observation

Fresh spleen tissues were fixed in 4% glutaraldehyde (Alfa Aesar, Germany) phosphate buffer (pH 7.4) at 4°C for more than 4 h. After flushing with 0.1 M of phosphate buffer (pH 7.4), the tissues were fixed again in 1% buffered osmium tetroxide solution (SPI-CHEM, USA) for 2 h. In the next stage, the samples were washed in phosphate buffer and dehydrated in an acetone series. Dehydrated tissues were embedded in epoxy resin (SPI-VHEM, USA). Resin polymerization was conducted at 60°C for 36 h. The ultrathin sections (50~60 nm) were stained with uranyl acetate (Polyscience, USA) and citrate lead (Sigma Aldrich, USA). The ultrastructure was observed by TEM (Hitachi H7650, Japan).

Protein extraction and digestion

Spleen tissues from different periods were ground (1 M pH 6.8) in a mortar containing a protease inhibitor cocktail (Roche, Mannheim, Germany) and centrifuged (4°C, 12,000 × *g*, 15 min). The supernatant was collected, and tris-saturated phenol (pH 7.8) was added, followed by centrifugation (4°C, 12,000 × *g*, 15 min). After removing the supernatant, an equal volume of 50 mM Tris-HCl (pH 8.0) was added, followed by centrifugation (4°C, 12,000 × *g*, 20 min). After removing the supernatant, an equal volume of 50 mM Tris-HCl (pH 8.0) was added, followed by centrifugation (4°C, 12,000 × *g*, 20 min). After removing the supernatant, 0.1 M ammonium acetate was added to precipitate the protein at –20°C overnight. The mixture was centrifuged (4°C, 12,000 × *g*, 20 min), the protein pellet was washed with methanol twice, and the extracted proteins were lyophilized and stored at –80°C. The protein samples were then subject to alkylation for cysteine carbamidomethylation. After the protein was digested with trypsin (1:20 w/w, Promega, USA), the peptides were desalted with C18 SPE (CNW®, China) according to manufacturer's instructions. The concentrations of the peptides obtained after trypsin digestion were determined using a BCA Protein Assay kit (Pierce Biotechnology). After normalizing the concentrations of the samples, the enzyme efficiency was monitored by LC-MS (consists of UPLC M-Class system (Waters, USA) and Q Exactive HF (Thermo Fisher, USA) mass spectrometer). A total of 4 biological replicates were performed in this experiment.

Phosphopeptide enrichment

The workflow for phosphopeptide enrichment and quantitative analysis is shown in Fig. 1. Aliquots of TiO_2 (GL Sciences, Japan) beads were washed 3 times using buffer with 50% acetonitrile (ACN) containing 2% trifluoroacetic acid (TFA), saturated with glutamic acid. The TiO_2 beads and peptides were dissolved in 800 µl of the same buffer and gently shaken at room temperature for 1 h. The TiO_2 beads were then washed with 50% ACN to remove the non-phosphorylated peptides. Then, the TiO_2 beads were washed twice with 50% ACN containing 20 mM ammonium acetate. Phosphopeptides were then eluted from the TiO_2 beads with 200 µl of 0.3 M NH_4OH 1 time and with 200 µl of 0.5 M NH_4OH 2 times. The enriched phosphopeptides were then lyophilized and frozen at –20°C for subsequent use. A total of 4 biological replicates were performed in this experiment.

High-pH RP-HPLC for peptide separation

Each sample comprised an equal mixture of digested peptides. The mixture was then separated into ten eluted components by high-pH reversed phase high-performance liquid chromatography (RP-HPLC) (Waters e2695, USA) through a Durashell-C18 column (5-µm particle size, 100-Å pore size, 4.6 mm × 250 mm, Agela, China). The liquid phase separation gradient was as follows: 2% solvent B (100% ACN containing 5 mM ammonium formate, pH 10.0) and 98% solvent A (100% water containing 5 mM ammonium formate, pH 10.0) for 10 min, followed by 2~50% solvent B in 70 min, at a flow rate of 1 ml/min using a linear gradient. Each elution component was collected every 1 min, and a total of 60

elutions were collected. Every ten elutions were mixed together (i.e., 1, 11, 21, 31, 41, 51). Then, the samples were dried and stored at −80°C.

DDA spectral library construction

DDA spectral library construction was performed as previously described (Liam et al., 2019). Briefly, groups of ten samples were separated by liquid chromatography, then resuspended in a 0.1% formic acid water solution containing iRT reagent (Spectronaut, Switzerland), and then further analysed by LC-MS (consists of UPLC M-Class system (Waters, USA) and Q Exactive HF (Thermo Fisher, USA) mass spectrometer). Each sample was first loaded onto a C18 RP trap column (5-μm particle size, 100-Å pore size, 180-μm ID × 20-mm length; Waters, USA) and then separated on a C18 RP analytical column (1.8-μm particle size, 100-μm ID × 150-mm length; Waters, USA) at a flow rate of 300 nL/min using a linear ACN gradient of 2~8% solvent B in 6 min and then 8~35% solvent B in next 114 min (solvent A: 99.9% H2O, 0.1% formic acid; solvent B: 99.9% ACN, 0.1% formic acid). The sample was electrosprayed into the Q Exactive HF (2.0 kV and 290°C). The Q Exactive HF parameters were set as previously described [10]. The process of DDA data collection for enrichment of phosphopeptides was the same as described above. Proteome Discoverer (version 2.2, Thermo Fisher Scientific) was used to search the DDA mass spectrometry results for the above groups of 10 samples in order to construct DDA spectral libraries. The database was derived from the protein sequences for Mus musculus downloaded from UniProt (2017/12/07, 16944 sequences), and trypsin, human keratins, and *Babesia* sequences were used as contaminated database. Data search parameters were set as previously described [10].

DIA spectral acquisition and data analysis

DIA analysis was carried out for each sample. The chromatographic conditions for DIA were the same as those for DDA spectral library construction. The DIA mass spectrometry parameters were as follows: (a) DIA mode; scanning range for a full scan, 350~1200 m/z; resolution of the precursor ion, 60,000; automatic gain control (AGC) target, 3×10^6; and maximum ion injection time (maximum IT), 50 ms; (b) HCD normalized collision energy, 27%; (c) DIA MS2 scanning, 34 consecutive windows, each of which was set to 26 m/z and a 1 m/z overlap between 2 adjacent windows; and (d) MS2 scan resolution, 30,000; AGC target, 1×10^6; and maximum IT, set to auto.

DIA data were analysed using Spectronaut software (Version 11.0, Switzerland). The default parameters for DIA data analysis were used, where the FDR for proteins and peptides was set to less than 1%. The protein expression levels in all treatment groups were compared with the control group, and the ratio was regarded as the change in protein or peptide expression, which was also the basis for further data analysis and discussion. Proteins quantified with at least 2 unique peptides and whose Q value <0.05 and expression change times >1.5 were considered to have significant changes in expression. For phosphopeptides, we only focused on the quantitative phosphopeptide results. If the change in phosphopeptides was more than 1.5 times, the degree of phosphorylation modifications was considered changed.

Bioinformatics analysis

Bioinformatics analysis was performed for all differentially expressed proteins or phosphopeptides. Proteins with similar expression characteristics were clustered with GProX (Rigbolt et al., 2011). The number of clusters was set to 4, and a fixed regulation threshold (upper limit of 0.58 for protein upregulation and lower limit of −0.58 for protein downregulation, corresponding to the original ratios 1.5 and 0.67) was used. Principal component analysis (PCA) was performed with online analysis software (http://www.omicsolution.org/wu-kong-beta-linux/main/). PANTHER software (http://pantherdb.org/) was used for Gene Ontology (GO) functional categories. Pathways associated with the differentially expressed proteins were identified using the Kyoto Encyclopedia of Genes and Genomes (KEGG) database (http://www.kegg.jp/kegg/). The tool used for KEGG analysis was KEGG Mapper (https://www.kegg.jp/kegg/tool/map_pathway2.html).

Results

Effects of *B. microti* infection on the spleen

Morphological changes in the spleen at different time points after *B. microti* infection are shown in Fig. 1. Further amplification using TEM (Hitachi H7650, Japan) showed that normal mouse splenocytes had a clear mitochondrial cristae structure. After *B. microti* infection, the mitochondria in splenocytes exhibited abnormalities. On 19 d after infection, abnormal mitochondria gradually returned to a normal status (Fig. 2).

Identification and quantification of global proteins and phosphopeptides

The whole experimental design is shown in Fig. 1. The quantitative results for global proteins in all groups identified by mass spectrometry were analysed using Spectronaut 11 software. The numbers of identified proteins in mice in the normal group (0 d) and after 5 d, 8 d, 11 d, and 19 d of *B. microti* infection were 2804, 2890, 2888, 2936, and 2918, respectively; the numbers of proteins that had a coefficient of variation (CV) value lower than 20% among 4 biological repeats in all groups were 2250, 2214, 2270, 2425, and 2241, respectively. PCA was performed on data in 4 repeats for these 5 periods (Fig. 3A). The figure shows that the similarity among repeated data in all groups was high, indicating that the reproducibility of the data in 4 repeats was high, while the 5 groups of data for the different infection periods were significantly different. The identified results were subject to Venn diagram analysis (Fig. 3B). The numbers of proteins that were identified in all 5 periods was 1403, of which 966 proteins were differentially expresses. The information for intersecting proteins is provided in Table S1. The mass spectrometry proteomics data have been deposited in the ProteomeXchange Consortium via the iProX partner repository (accession No. : IPX0002204000/PXD019236).

The quantitative results for phosphopeptides in all groups identified by mass spectrometry were analysed using Spectronaut 11 software. The numbers of identified phosphopeptides in mice in the normal group (0 d) and after 5 d, 8 d, 11 d, and 19 d of *B. microti* infection were 12373, 12689, 12792, 12670, and

12501, respectively; the numbers of phosphopeptides that had a CV value lower than 20% among 4 biological repeats in all groups were 5363, 8638, 9746, 6725, and 8042, respectively. PCA was performed on data in 4 repeats for these 5 periods, and the Venn diagram indicates that that there were 2261 intersecting phosphopeptides in the 5 periods (Figure S1). These 2261 phosphopeptides included 2470 phosphorylation modification sites, of which 2065 peptides contained 1 phosphorylation site, 183 peptides contained 2 phosphorylation sites, and 13 peptides contained 3 phosphorylation sites (Fig. 4A). Among 2470 phosphorylation sites, 82.19% occurred at serine residues, 16.11% occurred at threonine residues, and 1.70% occurred at tyrosine residues (Fig. 4B). When the mass spectrometry identification results of the same polypeptide in different periods had a fold change greater than 1.5, the peptide was considered to have differentially changed; in other words, the level of phosphorylation modification at this site changed. A total of 2169 phosphopeptides, corresponding to 1011 proteins, showed differences in mass spectrometry identification results. The information for intersecting phosphopeptides is provided in Table S2. The mass spectrometry proteomics data have been deposited in the ProteomeXchange Consortium via the iProX partner repository (accession No. : IPX0002209000/ PXD019319).

Cluster analysis and GO annotation analysis of differentially expressed proteins

For the periods of 5 d/0 d, 8 d/0 d, 11 d/0 d, and 19 d/0 d of *B. microti* infection, cluster analysis was performed on 1403 intersecting proteins that had annotation information (Fig. 5). These proteins were grouped into 5 clusters when the log2 value was > 0.58 or < −0.58. The results showed that Cluster 0 had 437 proteins with differential expression level changes that were not significant. Cluster 1 had 225 proteins, and the expression levels of these proteins were upregulated with the increase in the infection rate; however, the expression levels of these proteins slightly decreased with recovery at 19 d. Functions of these proteins were associated with defending against *B. microti* infection. Cluster 2 had 269 proteins. The expression levels of these proteins were downregulated on 5 d, 8 d, and 11 d after infection and upregulated on 19 d. Cluster 3 had 244 proteins. The expression levels of these proteins were upregulated on 5 d, 8 d, and 11 d after infection and downregulated to normal levels on 19 d. Cluster 4 had 228 proteins. Their expression levels were downregulated on 5 d of infection and gradually upregulated on 8 d, 11 d, and 19 d.

Proteins in Cluster 1~Cluster 4 that exhibited expression changes were subject to GO annotation analysis (Fig. 6). These proteins were classified into the following categories: Biological Process, Cellular Component, and Molecular Function. Proteins in Cluster 1 in the Biological Process category were further enriched in 8 nodes. The percentages of proteins in the cellular process (53.4%) and metabolic process (51.1%) nodes were high. Proteins in the Cellular Component category were further enriched in 4 nodes. The percentages of proteins in the cell part (54.9%) and organelle (40.6%) nodes were high. Proteins in the Molecular Function category were further enriched in 5 nodes. The percentages of proteins in the binding (44.4%) and catalytic activity (27.8%) nodes were high.

Proteins in Cluster 2 in the Biological Process category were further enriched in 12 nodes. The percentages of proteins enriched in the cellular process (55.6%) and metabolic process (34.6%) nodes

were high. Proteins in the Cellular Component category were further enriched in 5 nodes. The percentages of proteins in the cell part (45.9%) and organelle (34.6) nodes were high. Proteins in the Molecular Function category were further enriched in 7 nodes. The percentages of proteins in the binding (39.8%) and catalytic function (34.6%) nodes were high.

Proteins in Cluster 3 in the Biological Process category were further enriched in 10 nodes. The percentages of proteins in the cellular process (60.1%) and metabolic process (57.2%) nodes were high. Proteins in the Cellular Component category were further enriched in 5 nodes. The percentages of protein in the membrane (53.6%) and macromolecular complex (39.1%) nodes were high. Proteins in the Molecular Functions category were further enriched in 8 nodes. The percentages of proteins in the catalytic activity (39.9%) and binding (37.7%) nodes were high.

The expression levels of proteins in Cluster 4 were downregulated on 5 d and gradually upregulated on 8 d, 11 d, and 19 d. The proteins in the Biological Process category were further enriched in 11 nodes. The percentages of proteins in the cellular process (47.7%) and metabolic process (42.3%) nodes were high. Proteins in the Cellular Component category were further enriched in 7 nodes. The percentages of proteins in the cell part (38.5%) and organelle (21.5%) nodes were high. Proteins in the Molecular Function category were further enriched in 6 nodes. The percentages of proteins in the catalytic activity (42.3%) and binding (20.8%) nodes were high.

Cluster analysis and GO enrichment analysis of differentially expressed phosphopeptides

For the periods of 5 d/0 d, 8 d/0 d, 11 d/0 d, and 19 d/0 d of *B. microti* infection, cluster analysis was performed on differentially modified phosphopeptides (Figure S2). A log2 value >0.58 indicated upregulation, showing that this peptide was upregulated and the phosphorylation modification level of this peptide was upregulated. A log2 value <−0.58 indicated downregulation, showing that this peptide was downregulated and the phosphorylation modification level of this peptide was downregulated. These proteins were grouped into 5 clusters. The results showed that the phosphorylation modification changes in 92 peptides in Cluster 0 were not significant. The phosphorylation modification levels of 560 phosphopeptides in Cluster 1 were upregulated with the increase in the infection rate. However, the modification levels were downregulated on 11 d when the infection rate decreased and then gradually returned to normal levels in the recovery period on 19 d. The modification levels of 547 phosphopeptides in Cluster 2 were downregulated on 5 d, 8 d, and 11 d after *B. microti* infection and upregulated on 19 d. The phosphorylation modification levels of 408 phosphopeptides in Cluster 3 were upregulated on 5 d and 8 d and returned to normal levels on 11 d and 19 d. The phosphorylation modification levels of 554 phosphopeptides in Cluster 4 were downregulated on 5 d, 8 d, and 11 d and upregulated again on 19 d.

GO annotation was performed on proteins corresponding to differentially expressed phosphopeptides in Cluster 1~Cluster 4 (Figure S3). These proteins were classified into the following categories: Biological Process, Cellular Component, and Molecular Function. Proteins corresponding to phosphopeptides in Cluster 1 in the Biological Process category were further enriched in 11 nodes. The percentages of proteins in the metabolic process (39.7%) and cellular process (38.0%) nodes were high. Proteins in the

Cellular Component category were further enriched in 4 nodes. The percentages of proteins in the cell part (30.6%) and organelle (24.0%) nodes were high. Proteins in the Molecular Function category were further enriched in 6 nodes. The percentages of proteins in the binding (31.4%) and catalytic activity (22.3%) nodes were high.

Proteins corresponding to phosphopeptides in Cluster 2 in the Biological Process category were further enriched in 11 nodes. The percentages of proteins in the cellular process (48.8%) and metabolic process (43.1%) nodes were high. Proteins in the Cellular Component category were further enriched in 5 nodes. The percentages of proteins in the cell part (38.2%) and organelle (30.1%) nodes were high. Proteins in the Molecular Function category were further enriched in 7 nodes. The percentages of proteins in the binding (36.6%) and catalytic function (29.3%) nodes were high.

Proteins corresponding to phosphopeptides in Cluster 3 in the Biological Process category were further enriched in 10 nodes. The percentages of proteins in the metabolic process (40.8%) and cellular process (35.5%) nodes were high. Proteins in the Cellular Component category were further enriched in 4 nodes. The percentages of proteins in the cell part (32.9%) and organelle (25.0%) nodes were high. Proteins in the Molecular Function category were further enriched in 6 nodes. The percentages of proteins in the binding (32.9%) and catalytic function (19.7%) nodes were high.

Proteins corresponding to phosphopeptides in Cluster 4 in the Biological Process category were further enriched in 10 nodes. The percentages of proteins in the cellular process (52.2%) and metabolic process (41.6%) nodes were high. Proteins in the Cellular Component category were further enriched in 6 nodes. The percentages of proteins in the cell part (37.2%) and organelle (22.1%) nodes were high. Proteins in the Molecular Function category were further enriched in 5 nodes. The percentages of proteins in the binding (44.2%) and catalytic activity (31.9%) nodes were high.

KEGG pathway analysis of differentially expressed proteins and phosphorylated proteins

KEGG signalling pathway analysis was performed on 966 differentially expressed proteins. A total of 288 signalling pathways were involved (Fig. 7); 153 proteins were involved in metabolic pathways, and 44 proteins were involved in ribosome biogenesis. The following pathways were also involved: mitogen-activated protein kinase (MAPK) signalling pathway, T cell receptor signalling pathway, and Amoebiasis pathway.

Proteins with different changing trends in the 4 clusters were also subject to KEGG signalling pathway analysis (Fig. 8). The results of the KEGG signalling pathway analysis for Cluster 2 and Cluster 4 are shown below. Expression levels of proteins in these 2 clusters had stable changing trends. In Cluster 2, 17 proteins were involved in the regulation of the actin cytoskeleton pathway, suggesting that *Babesia* infection in host cells might induce changes in the host cytoskeleton in the early stage. Furthermore, we focused on pathways related to immunity and growth and development. The results showed that 9 proteins were involved in the T cell receptor signalling pathway, 7 proteins were involved in the MAPK signalling pathway, and 6 proteins were involved in the apoptosis pathway. In Cluster 4, 6 proteins were

involved in the MAPK signalling pathway, and some proteins were involved in the iron metabolism pathway. These pathways play important roles in defending pathogen invasion in the body, regulating iron homeostasis, and regulating growth and development in the body.

KEGG signalling pathway analysis was performed on 1011 phosphorylated proteins with phosphorylation modification changes. The results showed that these proteins were involved in a total of 174 signalling pathways (Figure S4). Immune- and growth and development-related signalling pathways were enriched in different periods, indicating that immune regulation in the body plays important roles in the process of defending against *B. microti* infection. Related pathways that involve immunity and growth and development include apoptosis, ribosome, MAPK signalling, and T cell receptor signalling pathways, of which 14 proteins were involved in the apoptosis pathway, 13 proteins were involved in the T cell receptor signalling pathway, and 10 proteins were involved in the MAPK signalling pathway. In addition, proteins with different changing trends in the 4 clusters were also subject to KEGG signalling pathway analysis (Figure S5).

Discussion

The spleen is the largest immune organ in mammals [11] and plays substantial roles in the activation and control of immune responses in the body [12,13]. The spleen can kill a large number of invading pathogens during blood filtration and is the most important organ in the body for defending against *Babesia* infection [14,15]. *Babesia* infection causes a series of morphological and physiological changes, such as the enlargement and presence of brown pigment granules [16]. The results in this study showed that the mitochondria in splenocytes exhibited abnormalities after *B. microti* infection. These results indicated that the spleen suffered very serious damage. With the progression of time, *B. microti* was gradually cleared by the immune system in the body. We found that the structure of spleen on 19 d of infection gradually recovered to the normal state; for example, the spleen volume gradually decreased, mitochondria also returned to normal, with potential disease amelioration. Although babesiosis is a self-limiting disease [17], damage to the body by *B. microti* can be substantial from the perspective of degree of spleen injury during peak infection. If hosts have other underlying diseases at this point, host mortality will greatly increase.

To explore the molecular mechanisms underlying the response of mouse spleen to *B. microti* infection, DIA quantitative proteomics was performed to systemically study dynamic changes in expression levels of global proteins and protein phosphorylation modifications in spleen tissues of mice after *B. microti* infection and to investigate protein regulation strategies of the spleen in response to *Babesia* infection in order to provide molecular bases for more accurate diagnosis and effective treatment of babesiosis. The results showed that the differentially expressed proteins in the spleen after infection were mainly cathepsin, interferon-induced proteins, interleukin enhancing factors, transferrin receptor proteins, glutamate-cysteine ligase, serotransferrin, and growth factor receptor binding proteins. Proteins that exhibited phosphorylation modifications included MAPKs, protein kinases, and transcription factors. These differentially expressed proteins mainly participate in infection defence in the body, the induction

of apoptosis and autophagy, the regulation of iron metabolism, and cell proliferation and growth-related pathways.

Immune-related proteins

The quantitative proteomics results in this study showed that the expression of many immune-related proteins changed in mouse spleen during *B. microti* infection. These proteins included cathepsin D (CTSD), interferon-induced protein 44 (IFI44), interleukin-2 enhancer binding factor 2 (ILF2), interleukin enhancer-binding factor 3 (ILF3), and signal transducer and activator of transcription 5A (STAT5A). These proteins mainly participate in physiological activities such as protein degradation in lysosomes, autophagy, apoptosis, inhibition of excessive cell proliferation, and viral infection defence to ensure effective killing of *B. microti*.

After hosts are infected with common parasitic protozoans such as *Babesia*, *Plasmodium*, and *Leishmania*, lysosomes in host cells can engulf a large number of parasites [18-20]. CTSD belongs to the aspartic protease family. It is localized in lysosomes of various tissues and cells [21] and can participate in various physiological activities in cells including cell apoptosis [22], autophagy [23], and protein degradation [24]. Some studies have shown that CTSD degrades exogenous pathogens through the autophagy-lysosome system [23]. Furthermore, CTSD can also promote protein degradation in lysosomes to play a critical role in the process of antigen presentation [25]. This study showed that the expression level of CTSD was downregulated on 5 d and 8 d after *B.microti* infection and were upregulates after 11 d. After the mice were infected with *B. microti*, the cell structure in spleen was destroyed; in addition, the structure and morphology of organelles such as lysosomes also had abnormalities. We speculate that this might be the cause of the corresponding reduction in the expression level of CTSD in the early stage of infection. With the decrease in the degree of infection, the cell structure in mouse spleen gradually returned to normal. At this time, lysosomes already engulfed a large number of *Babesia* and a large amount of CTSD was urgently needed for lysosomal degradation of *Babesia*. Therefore, the expression of level of CTSD was upregulated correspondingly.

IFI44 is an interferonssion oα/β-induced protein [26]. Studies have shown that IFI44 is a potential inflammatory factor and can defend against viral infection through the inhibition of viral transcription [27]. Furthermore, high IFI44 expression promotes the entry of viruses into the latent period and prevents the reactivation of viruses [26]. As an interferon-induced protein, IFI44 expression levels directly reflect IFN-α/β activity. IFN-α/β plays an important role in defending against infection from many parasites such as *Leishmania donovani* [28], *Plasmodium* [29], *Toxoplasma* [30], and *Trypanosome brucei* [31]. Therefore, it is speculated that IFI44 might have indirect anti-protozoan functions. This study showed that after mice were infected with *B. microti*, the expression level of IFI44 in the spleen was upregulated on 5 d and 8 d and was then gradually downregulated afterward. The expression level returned to a normal level after 19 d. Therefore, we speculate that IFI44 participated in spleen immune responses after *B. microti* infection and directly or indirectly exerted its biological functions to defend against *B. microti* invasion. With the gradual recovery of the body, the expression level of IFI44 gradually returned to normal. Although

the mechanism of involvement of IFI44 in defending against *B. microti* infection is currently still not very clear, IFI44 might be able to be used as a marker for screening *Babesia* infection.

IFLF2 and ILF3 are components of nuclear factor of activated T cells (NFAT) [32]. It has been shown that the downregulation of ILF2 expression levels inhibits cell proliferation [33], whereas the downregulation of IFL3 expression, in addition to the inhibition of cell proliferation, also inhibits cell migration and invasion and promotes cell apoptosis [34]. Some parasites such as *Babesia*, *Plasmodium*, and *Leishmania* can cause unlimited cell proliferation after infecting hosts to eventually cause diseases in hosts [35,36]. This study showed that after *B. microti* infection in mice, the expression of ILF2 and IFL3 in the spleen was downregulated; notably, the expression was downregulated to the lowest level on 11 d. The expression level returned to a normal level on 19 d. Therefore, we speculate that *B. microti* infection in mice might result in excessive cell proliferation; therefore, reduced expression levels of ILF2 and IFL3 were required to inhibit unrestricted cell proliferation and avoid cell lesions.

The quantitative proteomics results for phosphorylated proteins in the spleen showed that phosphorylation modifications of some proteins changed after the spleen was infected by *Babesia*. These proteins were activated through changes in their phosphorylation modifications; thus, the proteins participated in immune defence. STAT5 is an important transcription factor. STAT5 after phosphorylation modification can initiate target gene transcription to play a critical role in T cell proliferation and differentiation, thus participating in host immunomodulation [37]. The results of this study showed that the phosphorylation modification level of STAT5 in the spleen of mice after *B. microti* infection was upregulated on 8 d. We speculate that the main function of STAT5 activation was to promote T cell proliferation and differentiation [38] to ensure more T cells participated in immune responses. With the gradual disappearance of *Babesia* under the clearance function of host immunity, mouse spleen function and structure also gradually returned to normal on 19 d after infection, and the phosphorylation modification level of STAT5 also returned to a normal level. These results indicated that changes in the phosphorylation modification of STAT5 had important immune defence functions during the *Babesia* infection period, the synthesis of a large amount of proteins was not required, and the normal modification pattern rapidly returned to normal when it was not required in the body. This is a very energy-saving cascade signalling transduction process.

Iron metabolism-related proteins

The iron ion is one of the important trace elements for the maintenance of life activities in the body [39]. Iron deficiency or excess will both cause adverse effects on health [40,41]. It has been shown that iron deficiency affects systemic oxygen transport to cause iron deficiency anaemia to further cause cell death and inhibit body growth [42,43]. Excessive free iron promotes oxygen free radical production, causes lipid peroxidation, oxidative stress, and DNA damage, and eventually leads to cell death, influencing body growth [44,45]. To maintain iron element balance in the body, the body finely regulates iron absorption, transport, utilization, and storage. This series of regulation requires the involvement of many proteins.

The major involved proteins include lactoferrin, serotransferrin, transferrin receptor protein 1 (TfR1), and glutamate-cysteine ligase (GCL).

Many parasitic protozoans have the ability to influence iron metabolism in hosts such as *Plasmodium* and *Leishmania*. These parasites can uptake a large amount of iron ions in hosts to maintain their growth and propagation [46,47]. When parasites propagate, they utilize hosts to provide enough iron supplements. It has been shown that when the iron content in hosts is too high, protozoan propagation indeed will be promoted [48]. In contrast, when the iron content in hosts is low, the parasitic rate significantly decreases.

Lactoferrin is an important non-haem iron binding protein and participates in the regulation of iron homeostasis in the body [49]. In addition, as an immunomodulatory protein, lactoferrin has many functions, including anti-parasitic [50], anti-bacterial [51], anti-viral [52], and anti-inflammatory [53] actions. Lactoferrin participates in the host defence mechanism through 2 methods. The first method involves lactoferrin binding to iron in hosts so pathogens cannot acquire enough iron from host cells; therefore, their growth is blocked [54]. The other method involves lactoferrin directly interacting with pathogens to inhibit pathogen adsorption and invasion into target cells [52]. The results in this study showed that after *B. microti* infection in mice, the expression level of lactoferrin in splenocytes was downregulated during the infection period and upregulated during the recovery period. Therefore, we speculate that the reduction in the expression level of lactoferrin in the spleen in the infection period might be caused by the uptake of a large amount of iron in mice by *B. microti* to supply their growth needs. At this time, iron deficiency in the body caused excessive expression of iron transport-related proteins; therefore, a large amount of lactoferrin was not required. Thus, the expression level of lactoferrin decreased. However, with the extension of infection time, the iron content in hosts decreased dramatically. To maintain iron balance in the spleen during the recovery period, the uptake of iron by cells through various methods is needed. At this time, a large amount of lactoferrin proteins were required to assist in iron transport; therefore, the expression level of lactoferrin was upregulated.

Serotransferrin is a key protein involved in iron metabolism and in defending against microbial invasion in the body [55,56]. It can not only transport iron in the body in a soluble and non-toxic form to participate in iron metabolism [57] but can also inhibit the growth of pathogenic microorganisms through the clearance of free iron ions in hosts [56,58]. The results of this study showed that the expression level of serotransferrin in mouse spleen after *B. microti* infection was downregulated on 5 d and upregulated on 11 d. This regulation pattern for serotransferrin was similar to that for lactoferrin because they had similar functions in iron metabolism and anti-pathogen activities. They both have iron transport functions [59,60]. In addition, lactoferrin also has iron ion binding functions [50]. The coordinating regulation of these 2 proteins not only inhibited pathogen invasion in the body but also regulated iron balance in the body.

TfR1 distributes on the surface of mammalian cells to mediate the entry of iron taken up by transferrin from outside cells into cells [61]. It has been shown that the expression level of TfR1 is negatively

correlated with iron reserve in the body [62]. When iron is deficient in the body, cells increase iron intake through the expression of high levels of TfR1 [43]. In contrast, when iron is excessive, the expression level of TfR1 will decrease correspondingly to decrease iron intake [63]. This study showed that after mice were infected with *B. microti*, the expression level of TfR1 was significantly upregulated in mouse spleen and the fold upregulation peaked on 11 d. With the gradual recovery of the body on 19 d, the expression level of TfR1 also recovered to a normal level. Therefore, we speculate that the characteristics of expression changes in TfR1 mainly reflect a dramatic reduction in iron reserves due to the consumption of a large amount of iron ions in mouse splenocytes by *B. microti* after mice were infected with *B. microti*. To maintain iron ion homeostasis, cells had to express high levels of TfR1 to accelerate intracellular iron ion intake.

GCL is a rate-limiting enzyme of glutathione (GSH) synthesis [64]. It is a heterodimer composed of a modifier subunit (GCLM) and a catalytic subunit (GCLC) [65]. The results of this study showed that the expression of GCLM in mouse spleen on 5 d after *B. microti* infection was continuously upregulated and returned to a normal level on 19 d, whereas GCLC expression was upregulated on 11 d and returned to a normal level on 19 d. These results indicated that the GCL expression level increased correspondingly after splenocytes were infected with *B. microti*. With the decrease in the infection level of *B. microti*, the GCL expression level also returned to a normal level. Infection of hosts by some common parasitic protozoans usually causes abnormal levels of iron in hosts [48], promotes an increase in oxygen free radical levels in the body, and induces oxidative stress responses in the body [66]. GSH protects cells from oxidative damage [67], and the first step of GSH synthesis is catalysed by GCL [68]. Therefore, we speculate that the GCL expression level increased in the spleen after mice were infected with *B. microti* to effectively accelerate GSH biosynthesis. The presence of a large amount of GSH ensured high oxygen free radical clearance and antioxidant abilities [69] to maintain homeostasis in splenocytes.

Growth and development-related proteins

This study showed that the expression levels or phosphorylation modification levels of many proteins involved in growth and development changed in mouse spleen during *B. microti* infection. These proteins included protein kinase C-δ (PKC-δ), mitogen-activated protein kinase 3/1 (MAPK3/1), growth factor receptor-bound protein 2 (Grb2), and P21-activated kinase 2 (PAK2).

Protozoan infection usually causes uncontrolled host cell proliferation [70]. When the condition is severe, infection will even result in host organ failure until death. This condition is more common in babesiosis [71]. To prevent excessive cell proliferation, the host body will adopt an effective response mechanism. PKC-δ is a Ser/Thr-specific kinase and is involved in many basic cellular processes, including growth and differentiation [72]. It has been shown that under the function of many cytokines, including IFN-α, PKC-δ is activated by phosphorylation. Activated PKC-δ can inhibit cell proliferation and promote cell apoptosis [73,74]. This study showed that on 8 d and 11 d after *B. microti* infection in mice, PKC-δ expression in the spleen was not only downregulated but the phosphorylation modification level was also downregulated.

We speculate that this pattern of change in PKC-δ during the infection period prevented excessive proliferation of splenocytes during the *Babesia* infection period to avoid body damage.

MAPK is a protein kinase composed of Ser/Thr kinases [75]. The MAPK signal transduction pathway is linked with cell surface growth factors through Grb2 [76]. MAPK1 (also known as ERK2) regulates cell proliferation, survival, adhesion, and migration through the phosphorylation of hundreds of nuclear substrates and cytoplasmic substrates in cells [77]. MAPK3 (also known as ERK1) also plays a critical role in cell proliferation [78]. We found that the expression level of MAPK1 was slightly downregulated after *B. microti* infection and that the phosphorylation modification level was significantly downregulated on 11 d. Changes in the expression level of MAPK3 were not large; however, the phosphorylation modification level was significantly downregulated and the fold downregulation was the highest on 11 d. It has been shown that insufficient MAPK3/1 (ERK1/2) expression blocks cell proliferation [78,79]. Dephosphorylation of MAPK3/1 (ERK1/2) inhibits cell proliferation and differentiation [80]. In addition, this study showed that the expression level of Grb2 was downregulated after *B. microti* infection in mice and returned to a normal level on 19 d. The reduction in the Grb2 expression level reduced the abilities of various cytokines in response to the induction of proliferation signal transduction [81]. Therefore, we speculate that the regulation patterns of these MAPK signal transduction-related proteins in mouse spleen effectively inhibited the unrestricted proliferation of host cells during the infection period.

Babesia infection in host cells results in insufficient blood glucose in hosts [82]. PAK2 is an important participant in the insulin signalling pathway and glucose homeostasis [83]. It has been shown that the downregulation of PAK2 expression promotes glucose uptake [84]. This study showed that after *B. microti* infection in mice, the expression level of PAK2 in the spleen was downregulated on 8 d and 11 d and was close to a normal level on 19 d. We speculate that the blood glucose level decreased after *B. microti* infection in mice. Cells reduced PAK2 expression level to promote glucose uptake in order to maintain glucose homeostasis.

Conclusion

After the mice were infected with *B. microti*, their spleen were seriously damaged. However, spleen still initiated immune response to deal with the infection, in which immune-related proteins played an important role, including CTSD, IFI44, ILF2, ILF, and STAT5A. In addition, some proteins related to iron metabolism were also involved in the repair of spleen against *B. microti* infection, including serotransferrin, lactoferrin, TfR1, and GCL. At the same time, the expression and phosphorylation of proteins related to the growth and development of the spleen also changed, including PKC-δ and MAPK3/1, Grb2, and PAK2. All of the above proteins play an important important role in the regulation of spleen injury and maintenance of homeostasis.

Declarations

Acknowledgements

Thanks Institute of Laboratory Animal Sciences, Chinese Academy of Medical Sciences for donating *B. microti* in this experiment.

Author contributions

HW designed the experiments, XX wrote the initial manuscript. SR, AM, YH, XW, analyzed the data and performed experiments. MW, HL, XZ prepared the figures. JL designed the experiments and corrected the manuscript. All authors read and approved the final manuscript.

Funding

This work was supported by the Natural Science Fund for Distinguished Young Scholars of Hebei Normal University (No. L2017J04).

Availability of data and material

Data supporting the conclusions of this article are included within the article. The mass spectrometry proteomics data have been deposited in the ProteomeXchange Consortium via the iProX partner repository (Accession No. : IPX0002204000/PXD019236; No. : IPX0002209000/ PXD019319).

Ethics approval and consent to participate

Not applicable.

Consent for publication

Not applicable.

Competing interests

The authors declare no competing or financial interests.

References

1. Schnittger L, Rodriguez AE, Florin-Christensen M, Morrison DA. *Babesia*: a world emerging. Infect Genet Evol. 2012;12:1788-809.
2. Lobo CA, Cursino-Santos JR, Alhassan A, Rodrigues M. *Babesia*: an emerging infectious threat in transfusion medicine. PLoS Pathog. 2013;9:e1003387.
3. Vannier E, Gewurz BE, Krause PJ. Human babesiosis. Infect Dis Clin North Am. 2008;22:469-88.
4. Liu AH, Yin H, Guan GQ, Schnittger L, Liu ZJ, Ma ML, et al. At least two genetically distinct large *Babesia* species infective to sheep and goats in China. Vet Parasitol. 2007;147:246-51.
5. Fang DC, McCullough J. Transfusion-transmitted *Babesia microti*. Transfus Med Rev. 2016;30:132-8.

6. Bloch EM, Kumar S, Krause PJ. Persistence of *Babesia microti* infection in humans. Pathogens. 2019;8:102.
7. Golub R, Tan J, Watanabe T, Brendolan A. Origin and immunological functions of spleen stromal cells. Trends Immunol. 2018;39:503-14.
8. Ludwig C, Gillet L, Rosenberger G, Amon S, Collins BC, Aebersold R. Data-independent acquisition-based SWATH-MS for quantitative proteomics: a tutorial. Mol Syst Biol. 2018;14:e8126.
9. Xu B, Liu XF, Cai YC, Huang JL, Zhang RX, Chen JH, et al. Screening for biomarkers reflecting the progression of *Babes2ia microti* infection. Parasit Vectors. 2018;11:379.
10. Hawkins LJ, Wang MJ, Zhang BW, Xiao Q, Wang H, Storey KB. Glucose and urea metabolic enzymes are differentially phosphorylated during freezing, anoxia, and dehydration exposures in a freeze tolerant frog. Comp Biochem Physiol Part D Genomics Proteomics. 2019;30:1-13.
11. Li L, Duan MB, Chen WS, Jiang A, Li XM, Yang J, et al. The spleen in liver cirrhosis: revisiting an old enemy with novel targets. J Transl Med. 2017;15:111.
12. Lewis SM, Williams A, Eisenbarth SC. Structure-function of the immune system in the spleen. Sci Immunol. 2019;4:eaau6085.
13. Bronte V, Pittet MJ. The spleen in local and systemic regulation ofimmunity. Immunity. 2013;39:806-18.
14. Coleman JL, LeVine D, Thill C, Kuhlow C, Benach JL. *Babesia microti* and *Borrelia burgdorferi* follow independent courses of infection in mice. J Infect Dis. 2005;192:1634-41.
15. Genda J, Negron EA, Lotfipour M, Balabhadra S, Desai DS, Craft DW, et al. Severe *Babesia microti* infection in an immunocompetent host in Pennsylvania. J Investig Med High Impact Case Rep. 2016;4:2324709616663774.
16. Djokic V, Akoolo L, Parveen N. *Babesia microti* infection changes host spleen architecture and is cleared by a Th1 immune response. Front Microbiol. 2018;9:85.
17. Mathewson HO, Anderson AE, Hazard GW. Self-limited babesiosis in a splenectomized child. Pediatr Infect Dis. 1984;3:148-9.
18. Agbede RI, Kemp DH, Hoyte HM.
*Babesia bovis*infection of secretory cells in the gut of the vector tick *Boophilus microplus*. Int Parasitol. 1986;16:109-14.
19. Vijayan K, Cestari I, Mast FD, Glennon EKK, McDermott SM, Kain HS, et al. *Plasmodium* secretion induces hepatocyte lysosome exocytosis and promotes parasite entry. iScience. 2019;21:603-11.
20. Smirlis D, Dingli F, Pescher P, Prina E, Loew D, Rachidi N, et al. SILAC-based quantitative proteomics reveals pleiotropic, phenotypic modulation in primary murine macrophages infected with the protozoan pathogen *Leishmania donovani*. J Proteomics. 2020;213:103617.
21. Yu CP, Cha Y, Wu F, Xu XB, Qin L, Du M. Molecular cloning and functional characterization of cathepsin D from sea cucumber *Apostichopus japonicus*. Fish Shellfish Immunol. 2017;70:553-9.

22. Mehanna S, Suzuki C, Shibata M, Sunabori T, Imanaka T, Araki K, et al. Cathepsin D in pancreatic acinar Cells is implicated in cathepsin B and L degradation, but not in autophagic activity. Biochem Biophys Res Commun. 2016;469:405-11.
23. Suzuki C, Tanida I, Ohmuraya M, Oliva Trejo JA, Kakuta S. Lack of cathepsin D in the renal proximal tubular cells resulted in increased sensitivity against renal ischemia/reperfusion injury. Int J Mol. 2019;20:1711.
24. Benes P, Vetvicka V, Fusek M. Cathepsin D--many functions of one aspartic protease. Crit Rev Oncol Hematol. 2008;68:12-28.
25. Hausmann M, Obermeier F, Schreiter K, Spottl T, Falk W, Schölmerich J, et al. Cathepsin D is up-regulated in inflammatory bowel disease macrophages. Clin Exp Immunol. 2004;136:157-67.
26. Power D, Santoso N, Dieringer M, Yu J, Huang HC, Simpson S, et al. IFI44 suppresses HIV-1 LTR promoter activity and facilitates its latency. Virology. 2015;481:142-50.
27. DeDiego ML, Nogales A, Martinez-Sobrido L, Topham DJ. Interferon-Induced Protein 44 interacts with cellular FK506-Binding Protein 5, negatively regulates host antiviral responses, and supports virus replication. mBio. 2019;10:e01839-19.
28. Kumar R, Bunn PT, Sankar Singh S, Ng SS, de Oca MM, Labastida Rivera FD, et al. Type I interferons suppress anti-parasitic immunity and can be targeted to improve treatment of visceral leishmaniasis. Cell Rep. 2020;30:2512-2525.e9.
29. Yu X, Cai BW, Wang MJ, Tan P, Ding XL, Wu J, et al. Cross-regulation of two type I interferon signaling pathways in plasmacytoid dendritic cells controls anti-malaria immunity and host mortality. Immunity. 2016;45:1093-107.
30. Orellana MA, Suzuki Y, Araujo F, Remington JS. Role of beta interferon in resistance to *Toxoplasma gondi*i infection. Infect Immun. 1991;59:3287-90.
31. Lopez R, Demick KP, Mansfield JM, Paulnock DM. Type I IFNs play a role in early resistance, but subsequent susceptibility, to the African Trypanosomes. J Immunol. 2008;181:4908-17.
32. Lin HF, Shao JZ, Xiang LX, Wang HJ. Molecular cloning, characterization and expression analysis of grass carp (*Ctenopharyngodon idellus*) NF45 (ILF2) cDNA, a subunit of the nuclear factor of activated T-cells (NF-AT). Fish Shellfish Immunol. 2006;21:385-92.
33. Ni TT, Mao GX, Xue Q, Liu YF, Chen BY, Cui XF, et al. Upregulated expression of ILF2 in non-small cell lung cancer is associated with tumor cell proliferation and poor prognosis. J Mol Histol. 2015;46:325-35.
34. Hu XH, Dai J, Shang HL, Zhao ZX, Hao YD. SP1-mediated upregulation of lncRNA ILF3-AS1 functions a ceRNA for miR-212 to contribute to osteosarcoma progression via modulation of SOX5. Biochem Biophys Res Commun. 2019;511:510-7.
35. Lashnits E, Neupane P, Bradley JM, Richardson T, Thomas R, Linder KE, et al. Molecular prevalence of *Bartonella*, *Babesia*, and Hemotropic *Mycoplasma* species in dogs with hemangiosarcoma from across the United States. PLoS One. 2020;15:e0227234.

36. Schwing A, Pomares C, Majoor A, Boyer L, Marty P, Michel G. *Leishmania* infection: Misdiagnosis as cancer and tumor-promoting potential. Acta Trop. 2018;197:104855.
37. Orlova A, Wagner C, de Araujo ED, Bajusz D, Neubauer HA, Herling M, et al. Direct targeting options for STAT3 and STAT5 in cancer. Cancers (Basel). 2019;11:1930.
38. Wei L, Laurence A, O'Shea JJ. New insights into the roles of Stat5a/b and Stat3 in T cell development and differentiation. Semin Cell Dev Biol. 2008;19:394-400.
39. Abdizadeh H, Rana Atilgan A, Atilgan C. Mechanisms by which salt concentration moderates the dynamics of human serum transferrin. J Phys Chem B. 2017;121:4778-89.
40. Powell LW, Seckington RC, Deugnier Y. Haemochromatosis. Lancet. 2016;388:706-16.
41. Muckenthaler MU, Rivella S, Hentze MW, Galy B. A red carpet for iron metabolism. Cell. 2017;168:344-61.
42. Brissot P, Bernard DG, Brissot E, Loréal O, Troadec MB. Rare anemias due to genetic iron metabolism defects. Mutat Res. 2018;777:52-63.
43. Miyazawa M, Bogdan AR, Tsuji Y. Perturbation of iron metabolism by cisplatin through inhibition of iron regulatory protein 2. Cell Chem Biol. 2019;26:85-97.
44. Gozzelino R, Arosio P. The importance of iron in pathophysiologic conditions. Front Pharmacol. 2015;6:26.
45. Zhang C, Zhang F. Iron homeostasis and tumorigenesis: molecular mechanisms and therapeutic opportunities. Protein Cell. 2015;6:88-100.
46. Zhao H, Konishi A, Fujita Y, Yagi M, Ohata K, Aoshi T, et al. Lipocalin 2 bolsters innate and adaptive immune responses to blood-stage malaria infection by reinforcing host iron metabolism. Cell Host Microbe. 2012;12:705-16.
47. Malafaia G, de Nadai Marcon L, de Fátima Pereira L, Maria Lúcia P, Aparecida Rezende S. *Leishmania chagasi*: effect of the iron deficiency on the infection in BALB/c mice. Exp Parasitol. 2011;127:719-23.
48. Azcárate IG, Sánchez-Jaut S, Marín-García P, Linares M, Pérez-Benavente S, García-Sánchez M, et al. Iron supplementation in mouse expands cellular innate defences in spleen and defers lethal malaria infection. Biochim Biophys Acta Mol Basis Dis. 2017;1863:3049-59.
49. Mayeur S, Spahis S, Pouliot Y, Levy E. Lactoferrin, a pleiotropic protein in health and disease. Antioxid. Redox Signal. 2016;24:813-36.
50. Karav S, German JB, Rouquié C, Le Parc A, Barile D. Studying lactoferrin N-Glycosylation. Int J Mol Sci. 2017;18:870.
51. Buziashvili A, Cherednichenko L, Kropyvko S, Yemets A. Transgenic tomato lines expressing human lactoferrin show increased resistance to bacterial and fungal pathogens. Biocatal Agric Biotechnol. 2020;25:101602.
52. Ganz T. Iron and infection. Int J Hematol. 2018;107:7-15.
53. Conneely OM. Antiinflammatory activities of lactoferrin. J Am Coll Nutr. 2001;20:389-95, 396-7.

54. Sherman MP, Bennett SH, Hwang FFY, Yu C. Neonatal small bowel epithelia: enhancing anti-bacterial defense with lactoferrin and lactobacillus GG. Biometals. 2004;17:285-9.
55. Golizeh M, Lee K, Ilchenko S, Ösme A, Bena J, Sadygov RG, et al. Increased serotransferrin and ceruloplasmin turnover in dietcontrolled patients with type 2 diabetes. Free Radic Biol Med. 2017;113:461-9.
56. Lin L, Pantapalangkoor P, Tan B, Bruhn KW, Ho T, Nielsen T, et al. Transferrin iron starvation therapy for lethal bacterial and fungal infections. J Infect Dis. 2014;210:254-64.
57. Elsayed ME, Sharif MU, Stack AG. Transferrin saturation: a body iron biomarker. Adv Clin Chem. 2016;75:71-97.
58. Bruhn KW, Spellberg B. Transferrin-mediated iron sequestration as a novel therapy for bacterial and fungal infections. Curr Opin Microbiol. 2015;27:57-61.
59. Darmawan KK, Karagiannis TC, Hughes JG, Small DM, Hung A. High temperature induced structural changes of apo-lactoferrin and interactions with β-lactoglobulin and α-lactalbumin for potential encapsulation strategies. Food Hydrocoll. 2020;105:105817.
60. Choudhury D, Guha Thakurta P, Dasgupta R, Sen U, Biswas S, Chakrabarti C, et al. Purification and preliminary X-ray studies on hen serotransferrin in apo- and holo-forms. Biochem Biophys Res Commun. 2002;295:125-8.
61. Al-Refaei MA, Makki MR, Ali MH. Structure prediction of transferrin receptor protein 1 (TfR1) by homology modelling, docking, and molecular dynamics simulation studies. Heliyon. 2016;6:e03221.
62. Barisani D, Conte D. Transferrin receptor 1 (TfR1) and putative stimulator of Fe transport (SFT) expression in iron deficiency and overload: an overview. Blood Cells Mol Dis. 2002;29:498-505.
63. Wang B, Zhang JQ, Song F, Tian M, Shi BZ, Jiang H, et al. EGFR regulates iron homeostasis to promote cancer growth through redistribution of transferrin receptor 1. Cancer Lett. 2016;381:331-40.
64. Pereda J, Escobar J, Sandoval J, Luis Rodríguez J, Sabater L, Pallardó FV, et al. Glutamate cysteine ligase up-regulation fails in necrotizing pancreatitis. Free Radic Biol Med. 2008;44:1599-609.
65. Wiśniewski M, Lapiński M, Zdziarska A, Długosz E, Bąska P. Molecular cloning and analysis of *Ancylostoma ceylanicum* glutamate-cysteine ligase. Mol Biochem Parasitol. 2014;196:12-20.
66. Singh K, Ali V, Pratap Singh K, Gupta P, Suman SS, Ghosh AK, et al. Deciphering the interplay between cysteine synthase and thiol cascade proteins in modulating Amphotericin B resistance and survival of *Leishmania donovani* under oxidative stress. Redox Biol. 2017;12:350-66.
67. Yoshioka Y, Kadoi H, Yamamuro A, Ishimaru Y, Maeda S. Noradrenaline increases intracellular glutathione in human astrocytoma U-251 MG cells by inducing lutamate-cysteine ligase protein via β3-adrenoceptor stimulation. Eur J Pharmacol. 2016;5:51-61.
68. Raffa M, Hadj Jrad BB, Haj Khelil A, Kerkeni A, Mechri A. Association of polymorphism in glutamate-cysteine ligase catalytic subunit gene with schizophrenia: a case-control study in a Tunisian population. Gene Reports. 2016;4:249-52.

69. Tualeka AR, Martiana T, Ahsan A, Russeng SS, Meidikayanti W. Association between malondialdehyde and glutathione (L-gamma-Glutamyl-Cysteinyl-Glycine/GSH) levels on workers exposed to benzene in Indonesia. Open Access Maced J Med Sci. 2019;7:1198-202.
70. Dobbelaere DAE, Rottenberg S. *Theileria*-induced leukocyte transformation. Curr Opin Microbiol. 2003;6:377-82.
71. Bhanot P, Parveen N. Investigating disease severity in an animal model of concurrent babesiosis and Lyme disease. Int J Parasitol. 2019;49:145-51.
72. Slepchenko KG, Holub JM, Li YV. Intracellular zinc increase affects phosphorylation state and subcellular localization of protein kinase C delta (δ). Cell Signal. 2018;44:148-57.
73. Zhang DM, Fu MJ, Li LY, Ye H, Song ZQ, Piao TJ. PKC-δ attenuates the cancer stem cell among squamous cell carcinoma cells through down-regulating p63. Pathol Res Pract. 2017;213:1119-24.
74. Yanase N, Hayashida M, Kanetaka-Naka Y, Hoshika A, Mizuguchi J. PKC-δ mediates interferon-a-induced apoptosis through c-Jun NH 2 -terminal kinase activation. BMC Cell Biol. 2012;13:7.
75. Li XW, Tuergan M, Abulizi G. Expression of MAPK1 in cervical cancer and effect of MAPK1 gene silencing on epithelialmesenchymal transition, invasion and metastasis. Asian Pac J Trop Med. 2015;8:937-43.
76. Mitra P, Kalailingam P, Tan HB, Thanabalu T. Overexpression of GRB2 enhances epithelial to mesenchymal transition of A549 cells by upregulating SNAIL expression. Cells. 2018;7:97.
77. Garakani K, Shams H, Mofrad MRK. Mechanosensitive conformation of vinculin regulates its binding to MAPK1. Biophys J. 2017;112:1885-93.
78. Cao HY, Xiao CH, Lu HJ, Yu HZ, Hong H, Guo CY, et al. MiR-129 reduces CDDP resistance in gastric cancer cells by inhibiting MAPK3. Eur Rev Med Pharmacol Sci. 2019;23:6478-85.
79. Yang Y, Li XJ, Li P, Guo XT. MicroRNA-145 regulates the proliferation, migration and invasion of human primary colon adenocarcinoma cells by targeting MAPK1. Int J Mol Med. 2018;42:3171-80.
80. Ge J, Yan Q, Wang YJ, Cheng XQ, Song D, Wu C, et al. IL-10 delays the degeneration of intervertebral discs by suppressing the p38 MAPK signaling pathway. Free Radic Biol Med. 2020;147:262-70.
81. Frelin C, Ofran Y, Ruston J, Hayun M, Derdikman Y, Khier Y, et al. Grb2 regulates the proliferation of hematopoietic stem and progenitors cells. Biochim Biophys Acta Mol Cell Res. 2017;1864:2449-59.
82. Rees P, Schoeman JP. Plasma insulin concentrations in hypoglycaemic dogs with *Babesia canis rossi* infection. Vet Parasitol. 2007;152:60-6.
83. Varshney P, Dey CS. P21-activated kinase 2 (PAK2) regulates glucose uptake and insulin sensitivity in neuronal cells. Mol Cell Endocrinol. 2016;5:50-61.
84. Varshney P, Dey CS. Resveratrol regulates neuronal glucose uptake and insulin sensitivity via P21-activated kinase 2 (PAK2). Biochem Biophys Res Commun. 2017;485:372-8.

Figures

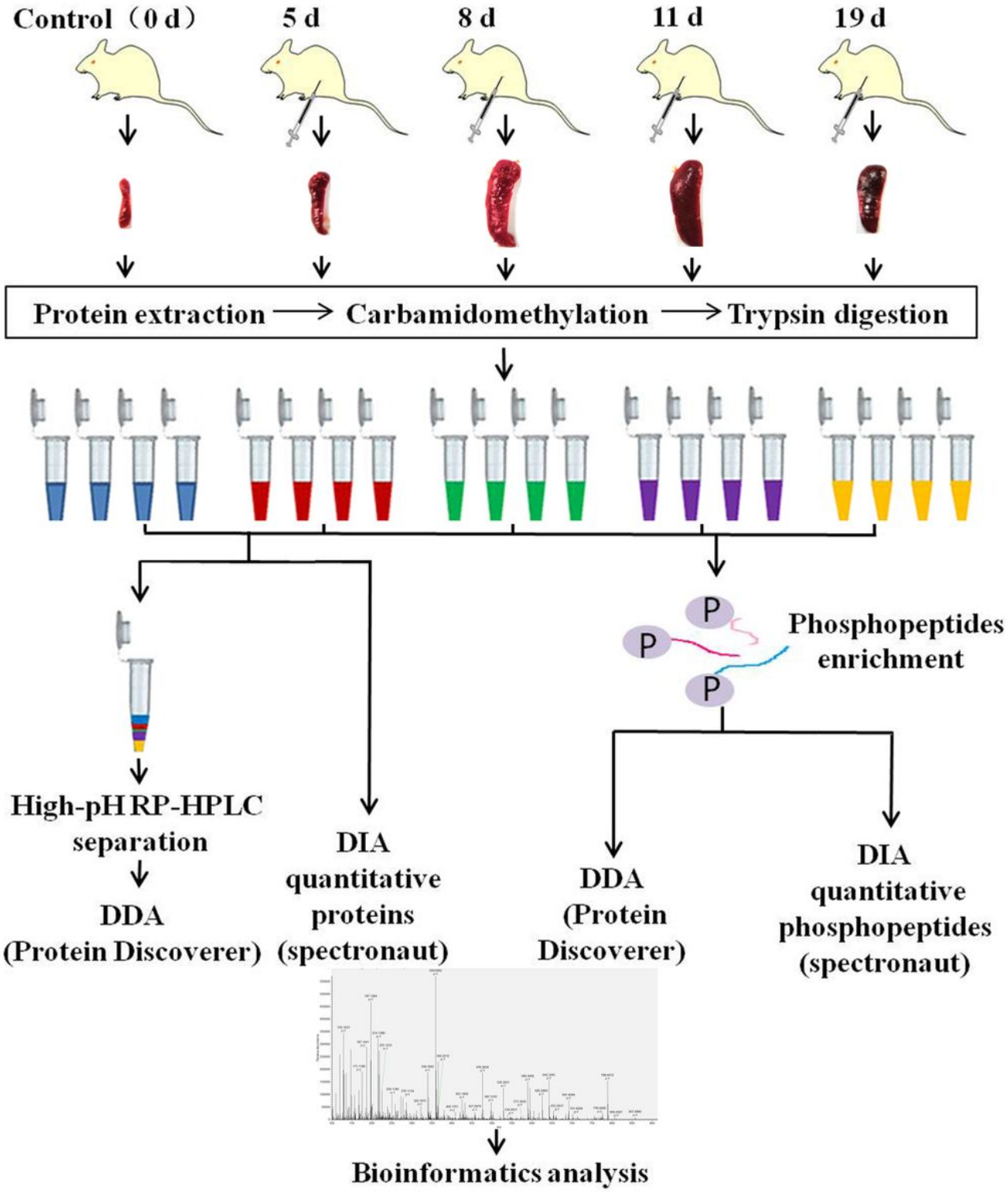

Figure 1

Whole experimental design for the proteomics analysis of global proteins and phosphorylated proteins in spleen tissue from mice infected with B. microti.

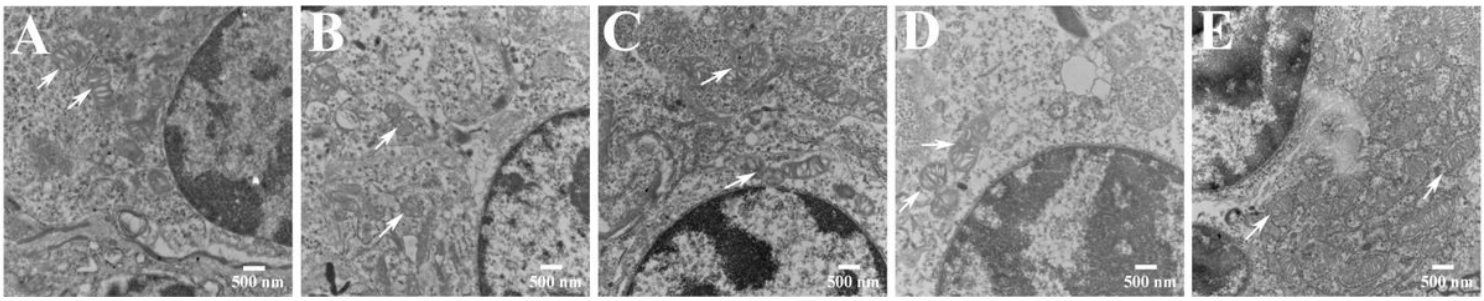

Figure 2

TEM observation of splenocytes in mice infected with B. microti at different stages. A: 0 d (control); B: 5 d; C: 8 d; D: 11 d; E: 19 d. Normal mouse splenocytes had a clear mitochondrial cristae structure. After 5 d, 8 d and 11 d of B. microti infection, the mitochondria of splenocytes exhibited abnormalities. After 19 d of infection, abnormal mitochondria slowly recovered to a normal status. Arrows indicate mitochondria.

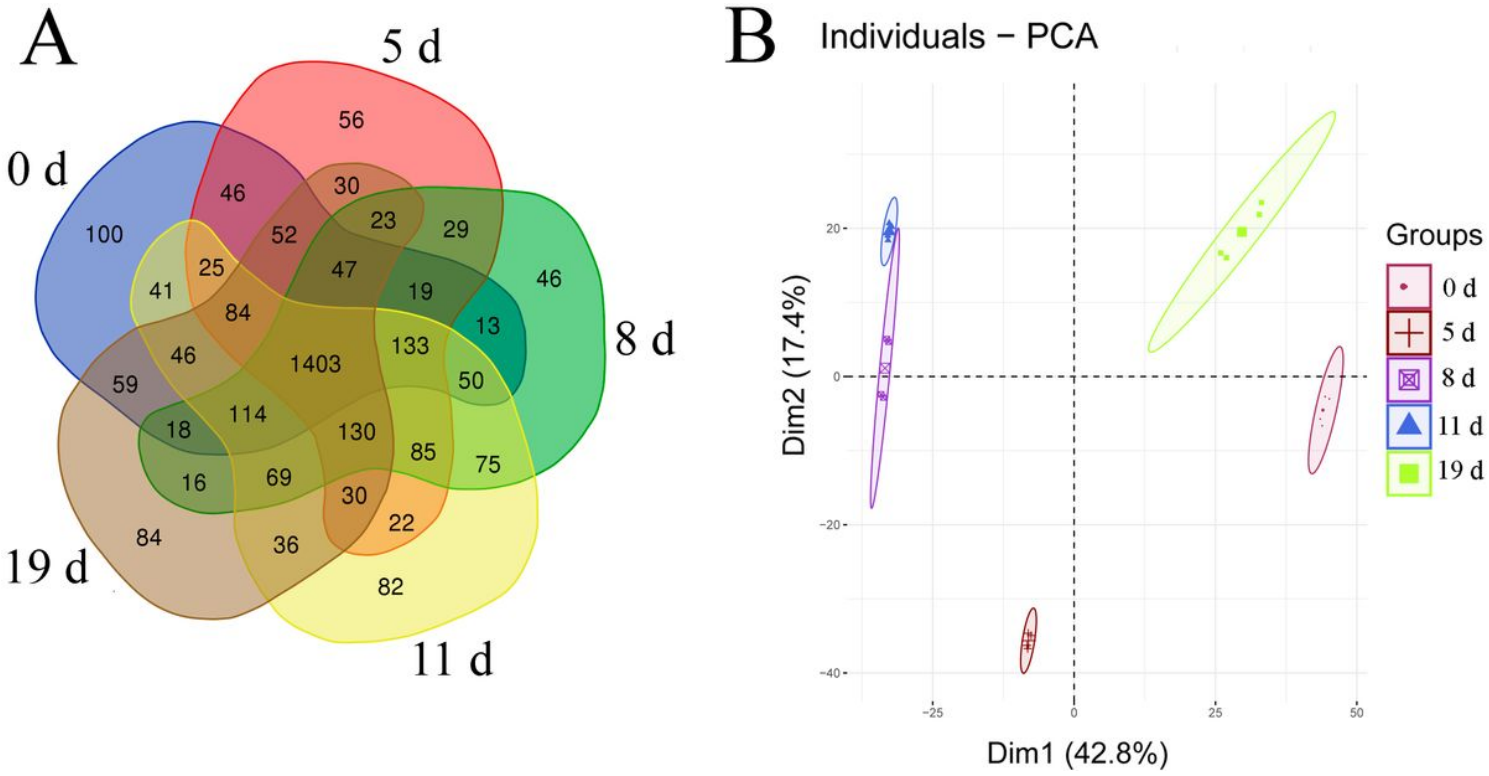

Figure 3

Statistics on the identified global proteins. (A) PCA of global protein mass spectrometry data at the five sampling times. (B) Venn diagram of proteins identified in various stages (global proteins).

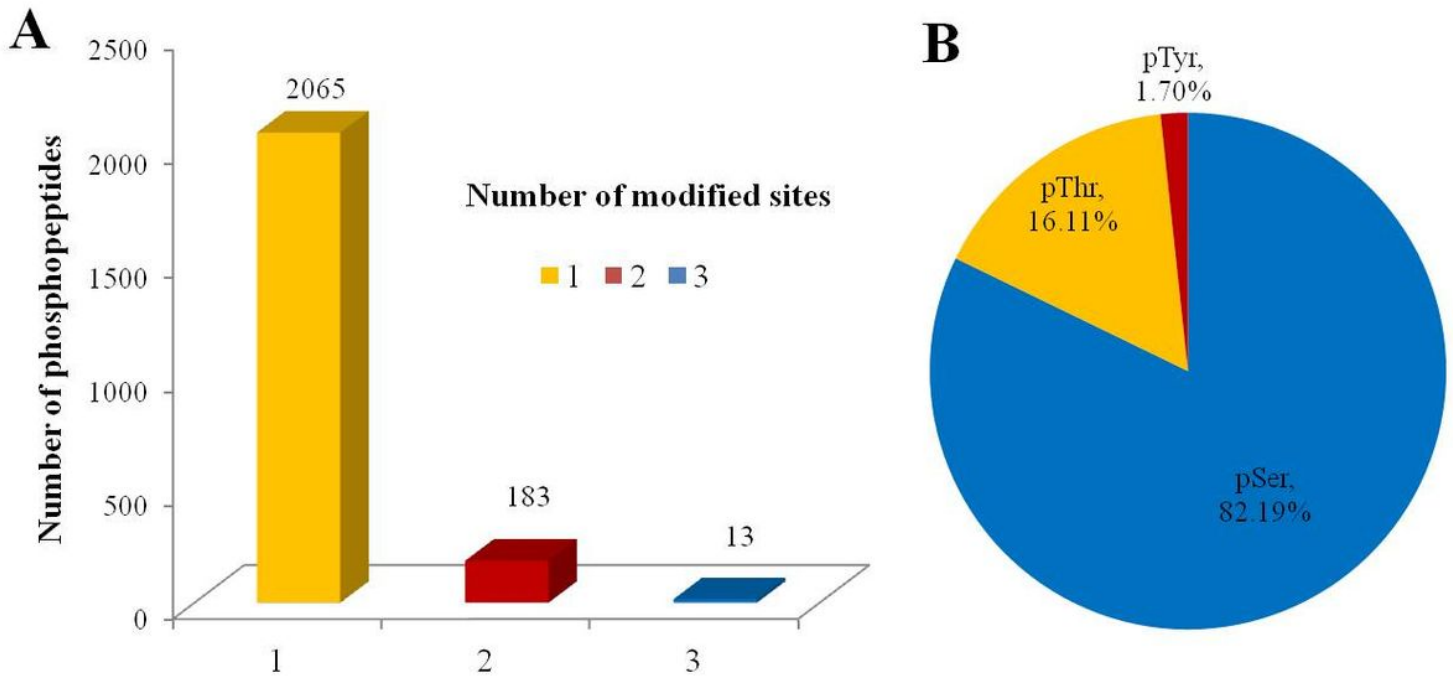

Figure 4

Statistics on the identified phosphorylated peptides. (A) Statistical analysis of the number of modification sites on phosphorylated peptide fragments. (B) Statistical analysis of percentages of the three types of amino acid phosphorylation.

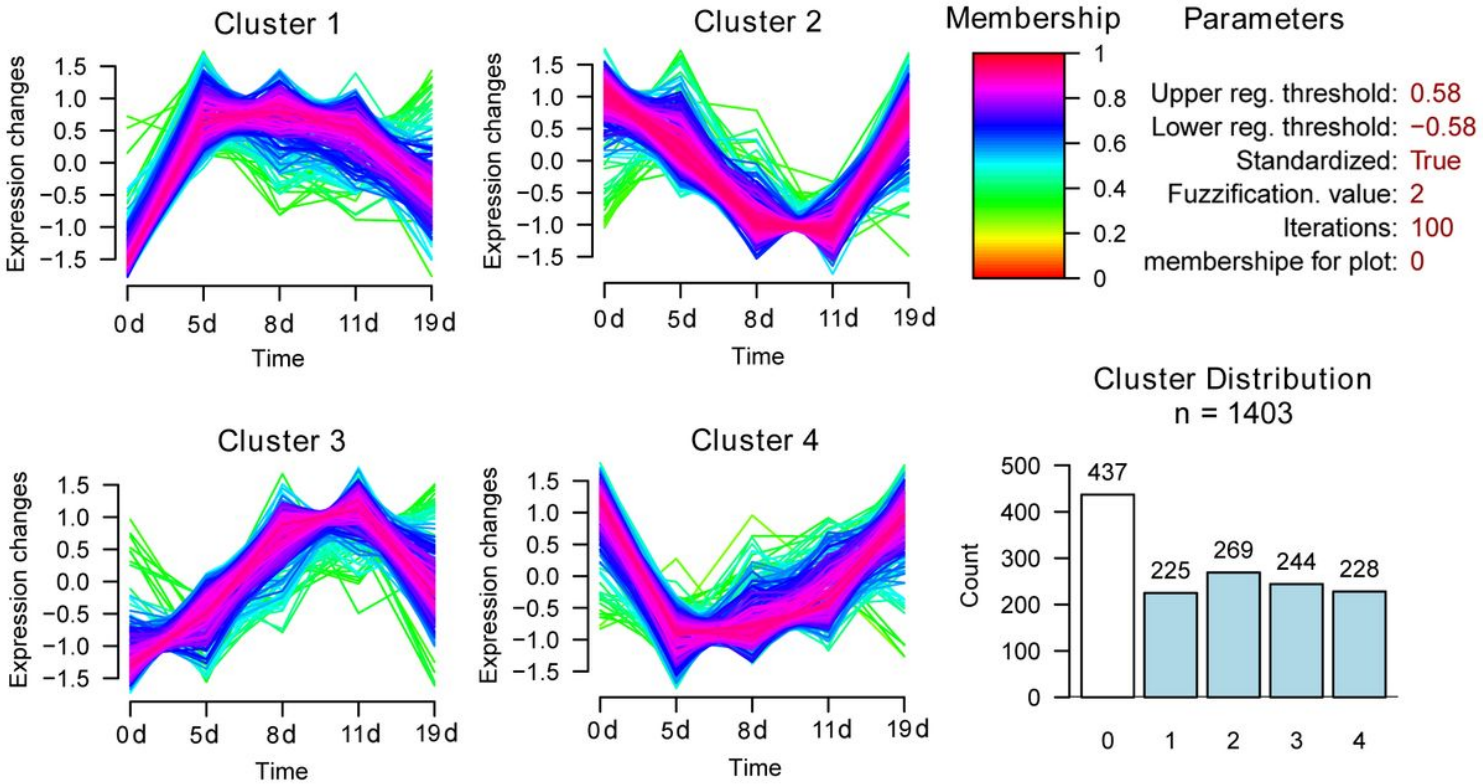

Figure 5

Cluster analysis of differentially expressed proteins in the spleen tissue of mice infected with B. microti.

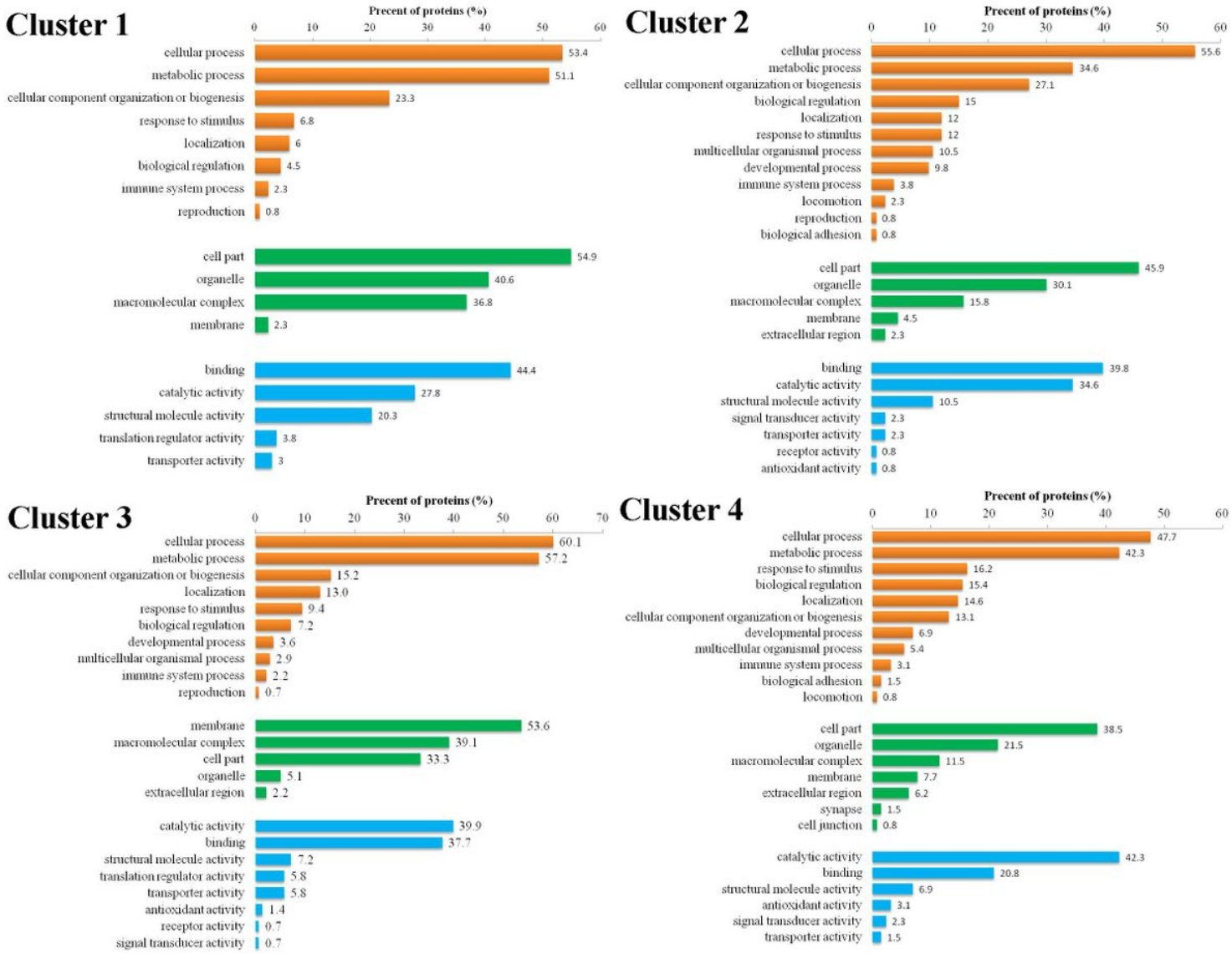

Figure 6

GO functional annotations of differentially expressed proteins in the four Clusters. MF: molecular function. BP: biological process. CC: cellular component.

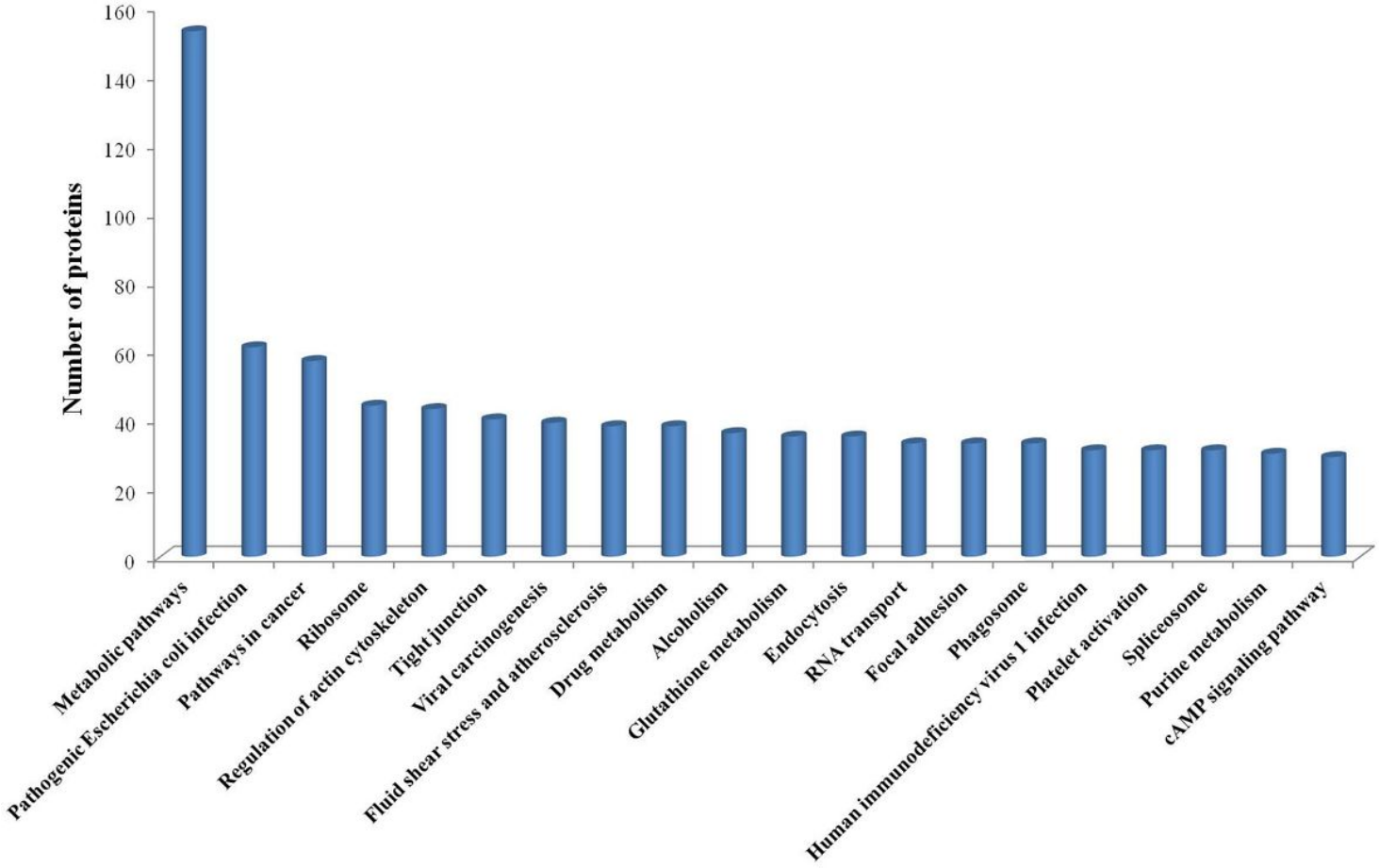

Figure 7

KEGG pathway analysis of differentially expressed proteins.

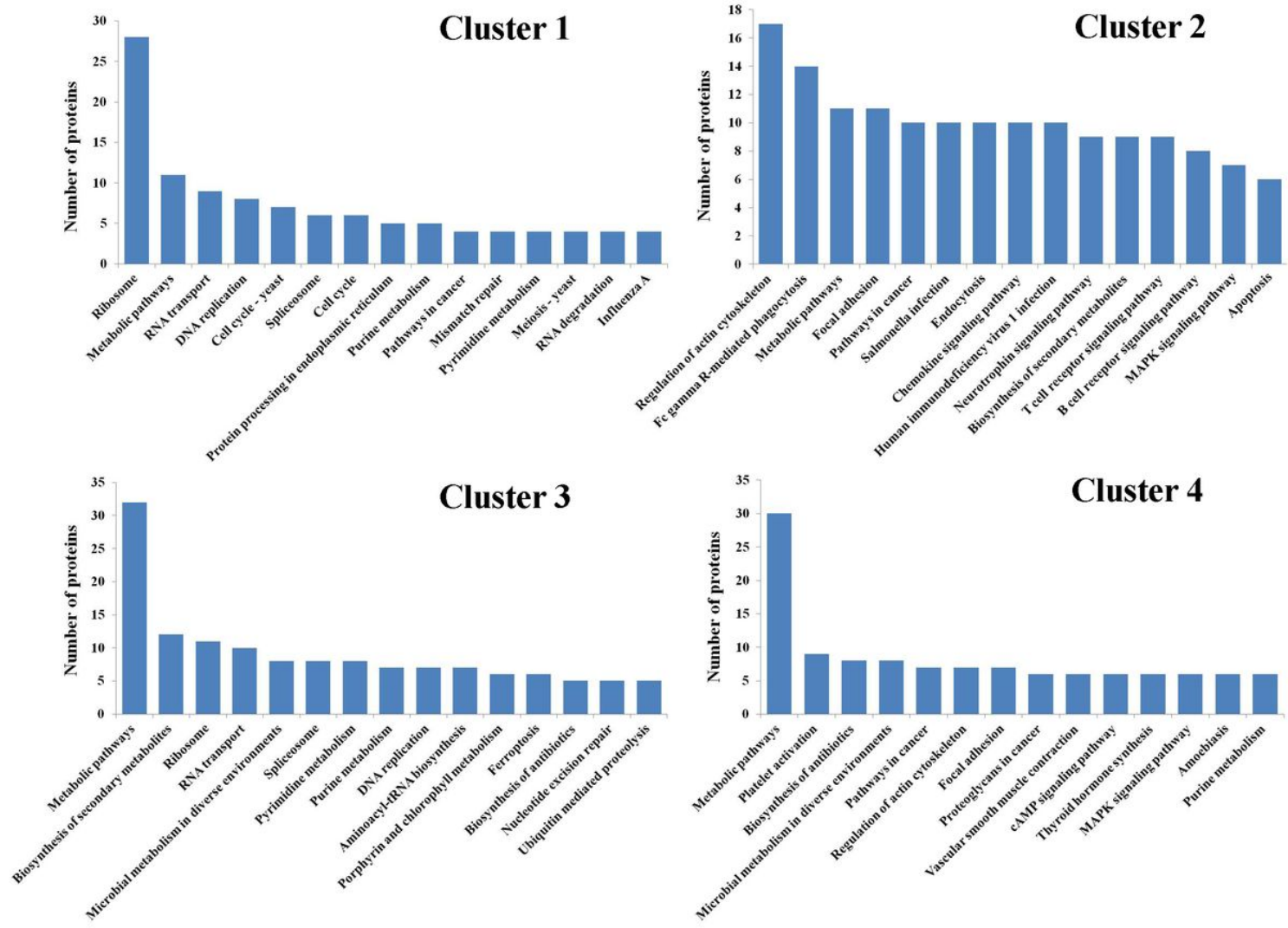

Figure 8

KEGG pathway analysis of the differentially expressed proteins in the four Clusters.

Supplementary Files

This is a list of supplementary files associated with this preprint. Click to download.

- supplement12.xlsx
- supplement13.xlsx
- supplement14.jpg
- supplement15.jpg
- supplement16.jpg
- supplement17.jpg
- supplement18.jpg